Appl Phys B (2009) 95: 399–405
DOI 10.1007/s00340-009-3490-3

Applied Physics B
Lasers and Optics

Photorefraction in $LiNbO_3$:Fe crystals with femtosecond pulses at 532 nm

D. Maxein · J. Bückers · D. Haertle · K. Buse

Received: 30 December 2008 / Published online: 3 April 2009

Abstract Photorefractive index gratings are written into iron-doped lithium niobate crystals using femtosecond laser pulses and cw light, both having a wavelength of 532 nm. The saturation value of the refractive index changes in as-grown samples is found to decrease with increasing peak pulse intensity. Furthermore, in oxidized crystals, writing with femtosecond pulses is much faster than with cw light and retains about the same writing speed than in as-grown crystals. We propose a charge transport model that addresses the special case of recording with high intensity femtosecond pulses.

PACS 77.84.Dy · 42.65.Hw · 72.20.Jv · 42.70.Ln

1 Introduction

The photorefractive effect in lithium niobate ($LiNbO_3$) crystals is, on the one hand, useful for, e.g., holographic applications such as wavelength filters and diffractive-optical elements [1], but on the other hand, light-induced refractive index changes can seriously affect, e.g., nonlinear-optical applications [2]: photorefraction can destroy the profile of an incoming light wave and can disturb the phase matching in nonlinear processes. Because of the impact of the photorefractive effect, over the last decades plenty of studies were performed in order to understand and to control the process. Most of these studies were done in the continuous wave (cw) regime. The increasing interest to use $LiNbO_3$ for high-intensity applications [3] is now generating demand to explore the photorefractive properties with femtosecond (fs) light pulses. Here we indeed refer to the "classical" photorefractive effect where a light-induced charge separation leads to space charge fields that modulate the refractive index through the electro-optic effect [4, 5], and not to effects like, e.g., Kerr gratings and other nonlinearities [6].

In some first studies, interesting photorefractive effects have already been discovered using femtosecond pulses and $LiNbO_3$ [7]: with fs pulses, writing of photorefractive structures is possible in $LiNbO_3$:Fe even at 1.5 μm wavelength, and the bulk photovoltaic current changes its sign when changing the writing light polarization. Pulse holography with $LiNbO_3$ has already been used for space–time conversion of optical information, so called "spectral holography" [8], and for data storage with microholograms [9].

To learn more about the photorefractive effect in $LiNbO_3$:Fe induced with fs pulses, we employ in this work for direct comparison pulses and cw light, both at a wavelength of 532 nm, to write elementary holographic gratings. The aim is to look for similarities and for differences in the photorefractive effect for pulsed and cw illumination.

2 Experimental setup

Femtosecond laser pulses of 532 nm are generated using a Clark MXR Inc. CPA2010 laser system and a subsequent optical parametrical amplifier TOPAS from LightConversion, Inc. The pulses have energies of about 70 μJ at a repetition rate of 1000 Hz, and FWHM pulse durations of about 160 fs. For direct comparison, a frequency-doubled Nd:YAG cw laser is available as an alternative light source of the same

D. Maxein (✉) · J. Bückers · D. Haertle · K. Buse
Institute of Physics, University of Bonn, Wegelerstraße 8, 53115 Bonn, Germany
e-mail: maxein@uni-bonn.de
url: http://www.photonik.uni-bonn.de/
Fax: +49-228-734038

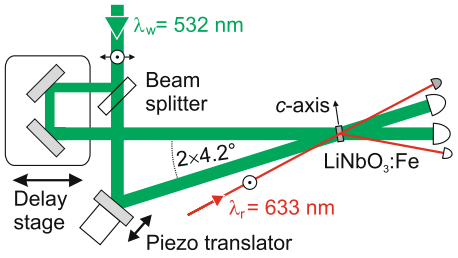

Fig. 1 Sketch of the setup used. Photorefractive gratings are written into $LiNbO_3$:Fe crystals at a writing wavelength of $\lambda_w = 532$ nm either with pulsed or cw light and are read out with cw light of the wavelength $\lambda_r = 633$ nm

wavelength. Unless otherwise noted, we provide the average intensity and power, both for the pulsed and the cw beam.

The beam passes a zero-order quartz wave plate and a Glan-laser polarizer. These elements define the polarization and provide a way of continuously attenuating the light power. It is then guided into the setup depicted in Fig. 1. A dielectric beam splitter (BS) provides two beams of approximately equal power. The beam reflected at the BS is further reflected at two silver mirrors mounted on a micrometer delay stage, before it hits the sample. The beam transmitted through the BS is reflected at a silver mirror, mounted on a piezoelectrically driven linear translator. Both beams interfere on the sample, the external angle between them is $2\theta_{\text{write}} = 8.4°$.

By changing the position of the micrometer stage, the optical length of one path can be adjusted to be equal to that of the other one. This is especially important for working with fs light pulses: since the pulses have a duration of less than 200 fs, the path lengths must coincide within a few µm. More precisely, due to their short duration and their relative angle, the pulses only interfere in a stripe of about 250 µm width [10], which is smaller than the geometrical beam diameter. By changing the delay, the stripe is shifted in the plane of the writing beams perpendicular to their bisector. During alignment, the delay is set such that the stripe lies in the center of the crystal. For measurements with cw light the interference pattern extends over the whole crystal width, since the coherence length is several cm.

To provide long-term stability of the interference pattern on the crystal, the setup is enclosed in a box to reduce air turbulences. In addition, drift of the components on a few-µm scale has to be compensated by active stabilization: to measure length changes between the two interferometer arms, an auxiliary cw laser beam is used. It is split at the BS and runs approximately parallel to the writing beams being reflected at the same mirrors. These two beams cross immediately below the crystal, where a gradient-index cylinder lens and the end of a fiber are positioned. The lens magnifies the interference pattern, and the end of the fiber is small enough to ensure that less than one fringe of the interference pattern is covered. Using a closed-loop control, this pattern is made stationary by adapting one arm length via the piezoelectric linear translator. This way, the optical path length difference between the two arms is kept constant on the sub-wavelength level.

Bragg-matched read-out of the emerging gratings in the crystal is done with an ordinarily polarized cw beam of 633 nm wavelength obtained from a HeNe laser. The beam is focused to about 100 µm FWHM beam waist with a 1500-mm lens. Since the beam is smaller than the interference stripe for fs pulse writing, a homogeneous grating in the read-out region can be assumed. The read-out beam is laterally (horizontally and vertically) adjusted to maximize the signal, i.e. to position it in the center of the interference stripe.

Behind the crystal, the transmitted and the diffracted read-out beam as well as the two writing beams are detected with silicon photodiodes. The transmitted (P_{trans}) and diffracted power (P_{diff}) of the read-out beam are used to calculate the diffraction efficiency

$$\eta = \frac{P_{\text{diff}}}{P_{\text{diff}} + P_{\text{trans}}}.$$

In transmission geometry and for Bragg-matched read-out, it is related to the amplitude of the refractive index changes Δn by [11]

$$\eta = \sin^2\left(\frac{\pi \Delta n\, d}{\lambda \cos\theta_{\text{B}}}\right),$$

where d is the thickness of the crystal, λ is the wavelength of the read-out light outside the crystal (633 nm), and θ_{B} is the angle between the read-out beam and the surface normal inside the crystal.

To erase the gratings, the crystals are illuminated homogeneously with the writing light and rotated ±3° relative to the writing position around the vertical y-axis for "off-Bragg" erasure. To obtain "writing light" without interference pattern, a 1-mm-thick glass plate is put in one of the arms delaying the corresponding pulses such that no interference occurs anymore, while for cw light one of the beams is simply blocked.

The samples are congruent lithium niobate crystals. We examined a nominally undoped $LiNbO_3$ as-grown crystal and crystals doped with iron ($LiNbO_3$:Fe) with a total iron concentration of $c_{\text{Fe}} = 20 \times 10^{24}\,\text{m}^{-3}$ in the as-grown as well as in the oxidized state. To oxidize the crystals, thermal annealing in oxygen was employed [12]. The concentration $c_{\text{Fe}^{2+}}$ of iron in the valence state 2+ is measured by absorption spectroscopy using the relation $c_{\text{Fe}^{2+}} = 2.16 \times 10^{21}\,\text{m}^{-1}\alpha_{477,\text{o}}$ [13], where $\alpha_{477,\text{o}}$ is the absorption constant at 477 nm for ordinary light polarization. This method yields an Fe^{2+} concentration $c_{\text{Fe}^{2+}}$ of $9 \times 10^{23}\,\text{m}^{-3}$ for the as-grown $LiNbO_3$:Fe crystal and an upper limit of $1.6 \times 10^{23}\,\text{m}^{-3}$ for the oxidized sample.

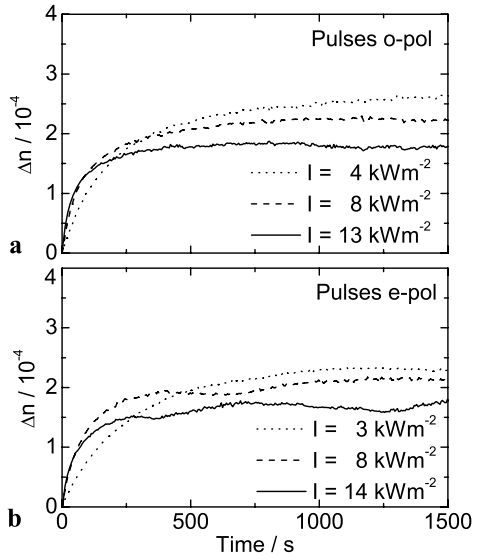

Fig. 2 Pulsed-light writing curves: refractive index changes induced in an as-grown $LiNbO_3$:Fe crystal (**a**) with ordinarily polarized pulses and (**b**) extraordinarily polarized pulses of different intensities

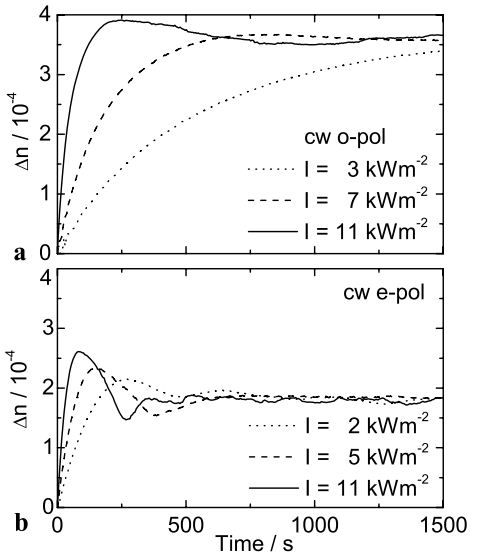

Fig. 3 Continuous-wave-light writing curves: refractive index changes induced in an as-grown $LiNbO_3$:Fe crystal (**a**) with ordinarily polarized cw light and (**b**) extraordinarily polarized cw light of different intensities

The crystals have the dimensions 0.5 × (0.8–1.2) × 1 mm^3 along x-, y-, and z-axes, respectively, where z is parallel to the c-axis of the crystal. The light propagates along x and is polarized parallel to y (o-pol) or z (e-pol). The writing beams have diameters of at least 1.5 mm FWHM; therefore the crystals are always illuminated homogeneously along the z-axis by each writing beam. The c-faces of the crystals are short-circuited with conductive silver paint to prevent a macroscopic charge buildup due to the bulk photovoltaic effect.

3 Results

3.1 As-grown crystals

First, we show in Figs. 2 and 3 typical writing curves, i.e. the temporal evolution of Δn, for pulses and cw light with different average intensities and different polarizations.

The refractive index changes Δn rise and finally reach a saturation level Δn_{sat}. While for pulses (Fig. 2) the curves are increasing monotonically, a maximum is observed for cw writing (Fig. 3) after which Δn decreases to the saturation value. This subsequent drop of Δn is more pronounced for extraordinarily polarized writing light and can be attributed to emerging "light-induced scattering", which was investigated previously [14] and which occurs on the same timescale than the observed decrease. Two other effects might play a minor role: complex writing time constants due to space charge limitation [4, 15] should not be pronounced for our Fe^{2+} concentration. Photorefractive phase coupling between the writing beams could be possible and partially responsible for the decrease after the maximum, although we did not observe any intensity beam coupling.

To quantify the writing curves, we fit the function

$$\Delta n(t) = \Delta n_{\mathrm{sat}}\left[1 - \exp(-t/\tau)\right]$$

to the data, which gives us the refractive index changes in saturation Δn_{sat} and the writing time constant τ. As it is known from literature, the reciprocal time constant τ^{-1} is proportional to the photoconductivity σ_{ph} [4, 5]. For cw illumination, a set of measurements covering only o-pol but a larger intensity range than the one shown in Fig. 3 is analyzed. Here, the fit is performed only until the first maximum in the curve is reached; since only o-pol measurements were analyzed, the maximum is less pronounced and hence has less influence on the fit compared to e-pol measurements. For an as-grown $LiNbO_3$:Fe crystal, the intensity dependences of Δn_{sat} and τ^{-1} are plotted in Fig. 4 for different measurement series with pulses and cw light. In the double-logarithmic plot of τ^{-1}, all series show a slope of 0.9 ± 0.1, i.e., the dependence is approximately linear. Additionally, the results for cw light and pulses are approximately equal, leading to similar proportionality constants between τ^{-1} and the average intensity I.

As can be seen in Fig. 4(b), Δn_{sat} is quite independent of the intensity for cw light. However, for pulses, there is a significant decrease of Δn for average intensities above 1 $kW\,m^{-2}$: for the two series of measurements using light pulses shown in this range, the actual parameters of the decrease are slightly different, but the trend is the same.

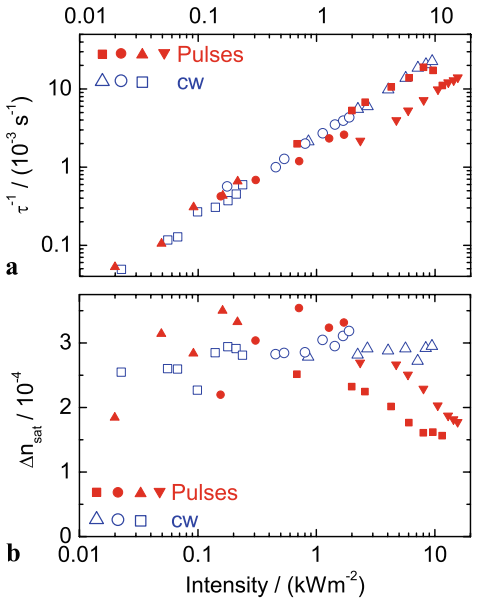

Fig. 4 Intensity dependences (**a**) of the inverse writing times τ and (**b**) of the saturation values of the refractive index changes Δn_{sat} for an as-grown $LiNbO_3$:Fe crystal illuminated with ordinarily polarized pulses (*closed symbols*) and cw light (*open symbols*). The different symbol shapes indicate the results of different measurement series

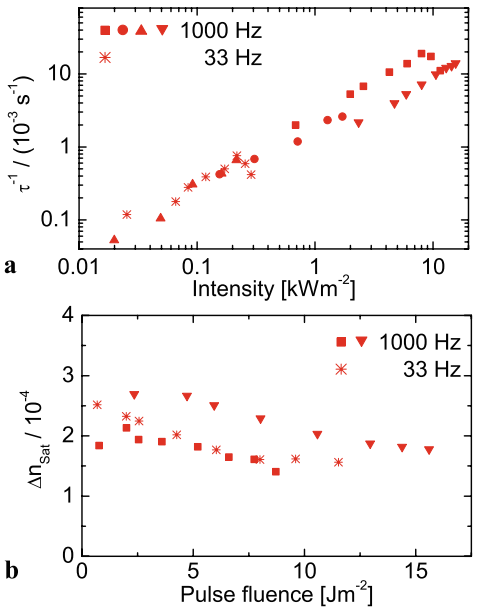

Fig. 5 Comparison of the relations (**a**) between the inverse writing times τ and the intensity, and (**b**) between the saturation values of the refractive index changes Δn_{sat} and the energy fluence per pulse for different pulse repetition rates of 1000 Hz and 33 Hz. The holograms are recorded in an as-grown $LiNbO_3$:Fe crystal with ordinarily polarized light. Different symbol shapes for 1000 Hz indicate the results of different measurement series

In order to check whether the average or the peak intensity is the real key parameter, the measurement is repeated with a pulse repetition rate of 33 Hz instead of 1000 Hz. In this way, just the average intensity I is decreased. The results are shown in Fig. 5: while the buildup speed τ^{-1} scales with the average intensity I, the decrease of Δn_{sat} is better described using the pulse fluence Φ_{Pulse} (energy per area per pulse), since the dependence of Δn_{sat} on the energy fluence Φ_{Pulse} is similar for both repetition rates.

In an undoped $LiNbO_3$ crystal no gratings at all could be found, regardless of using pulses or cw light for writing, even after illumination for several hours.

3.2 Oxidized crystals

Similar measurements are also performed in oxidized $LiNbO_3$:Fe. In Fig. 6, the writing curves for pulsed and cw light are plotted, but for different timescales: although the same average intensity is used, the grating is written about 50 times faster with pulses than with cw light.

For pulsed writing, the buildup times in oxidized and as-grown $LiNbO_3$:Fe are similar for the same intensities, as it can be seen in Fig. 7(a). For large I and therefore large Φ_{Pulse}, also the values of Δn_{sat} tend to be similar, while for small I they are larger in the as-grown sample, see Fig. 7(b).

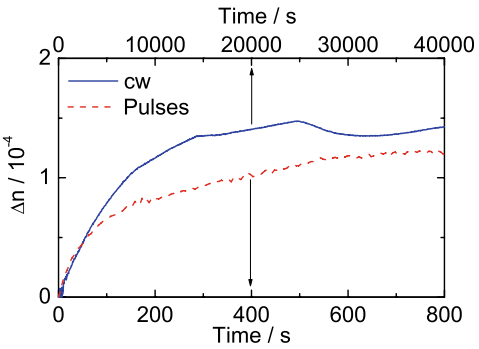

Fig. 6 Refractive index changes Δn induced in an oxidized $LiNbO_3$:Fe crystal versus recording time. Comparison of hologram recording with ordinarily polarized pulses (*dashed curve*) and cw light (*solid curve*) with average intensities of 4 kW m^{-2}

4 Discussion

4.1 Differences between fs and cw recording

Two main differences between recording with fs pulses and cw light become obvious.

(A) The Δn_{sat} values decrease with increasing pulse intensity. This does not only contradict the one-center model [16], which predicts an intensity independent Δn_{sat}, it is also inconsistent with the two-center model [17], which has been specifically developed for the high-intensity situation ($I > 10^4$ W m^{-2}) [18] and which assumes that the

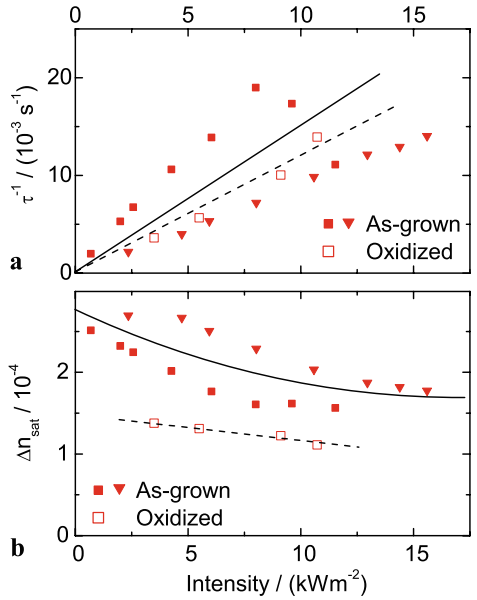

Fig. 7 Intensity dependence (**a**) of the inverse writing times τ^{-1} and (**b**) of the saturation values of the refractive index changes Δn_{sat} for an oxidized $LiNbO_3$:Fe crystal compared to those of an as-grown sample illuminated with ordinarily polarized pulses. The *lines* are just guides to the eye showing the dependences for the as-grown (*solid line*) and the oxidized (*dashed line*) samples. Different *symbol* shapes indicate the results of different measurement series

second centers are $Nb^{4+/5+}$ on Li site, $Nb_{Li}^{4+/5+}$, having a larger bulk photovoltaic coefficient than the deep $Fe^{2+/3+}$ centers [17]. Thus in order to explain $\Delta n_{sat}(I)$, we need an alternative model considering the special situation of ultra-high-intensity fs pulses.

(B) In oxidized crystals we can record holograms with an unexpected high speed—it is as high as that for writing in as-grown crystals. For cw recording, however, oxidization reduces the recording speed drastically, in accordance with predictions of the one-center model [16]. Again, a revised model is needed to address the case of fs recording.

In the following sections we will present a qualitative charge transport model which explains these differences. This model is summarized in Fig. 8: an electron excited by two-photon excitation (TPA) (1) is not subject to the bulk photovoltaic effect and therefore stays close to the position where it was excited. Here it has two possibilities: it can directly annihilate with a local hole (not depicted), or it can be trapped by Fe^{3+} or Nb_{Li}^{5+}, forming a photorefractive center Fe^{2+} or Nb_{Li}^{4+}, respectively (2). From there, the electron can take two ways: (a) it recombines with a local hole (not depicted). This process, like direct recombination from the conduction band, leaves the local charge density unchanged. (b) Instead, it can be re-excited by a photon and move to another position due the bulk photovoltaic effect (3), where it is (directly or indirectly) trapped by an Fe^{3+} ion, forming Fe^{2+} (4). From the migration of the electron, a local excess of holes results. Therefore, directly or indirectly, one local

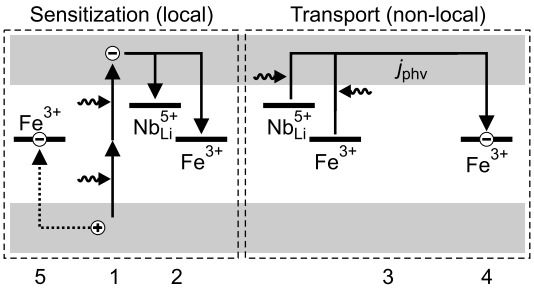

Fig. 8 Scheme of the charge excitation, migration, and trapping; see text

hole must recombine with a local, pre-existing Fe^{2+}, creating Fe^{3+} (5).

In the following we will have a closer look onto generation, migration, and final trapping of the charge carriers.

4.2 Additional charge generation by two-photon excitation

In the one-center model, electrons contributing to the photoconductivity σ_{ph} are created only by linear excitation from the Fe^{2+} levels into the conduction band, and their lifetime depends on the trap density. Therefore, σ_{ph} is proportional to the concentration ratio $c_{Fe^{2+}}/c_{Fe^{3+}}$ of Fe^{2+} and Fe^{3+} ions [4]. By oxidizing the crystals, $c_{Fe^{2+}}/c_{Fe^{3+}}$ is reduced from the initial value of about 0.1 by a factor of at least 5, with a very large error margin for the remaining small $c_{Fe^{2+}}$ value of the oxidized crystal. A ratio between the writing times of about 40, as observed for cw illumination, is therefore reasonable. But for pulses, the recording time constant hardly changes at all, i.e. σ_{ph} must be approximately the same. Thus, in the pulsed case, a further excitation mechanism must take place which is more or less independent of $c_{Fe^{2+}}$.

Because of the high peak intensities of fs pulses, two-photon absorption (TPA) exciting an electron from the valence band (VB) into the conduction band (CB) has to be considered. According to [19], the two-photon absorption coefficient for 532 nm wavelength is $\beta = 1.2 \times 10^{-3}$ m/GW. At the peak intensity of the pulses, this leads to an absorption coefficient of 140 m^{-1}, compared to a linear absorption coefficient of 285 m^{-1} in the as-grown crystals. One can guess that two-photon excitations bring the electrons higher into the conduction band increasing the quantum yield of electron–hole/trap separation. Thus it is feasible that the 140 m^{-1} nonlinear absorption can generate the same conductivity as the 285 m^{-1} linear absorption.

Counter-intuitively, TPA does not lead to a quadratic dependence of the photoconductivity σ_{ph} on I. The basic reason is the increasing number of holes (traps) and therefore the decreasing lifetime of the excited carriers. In [20] it is shown that a linear band-to-band excitation leads to a dependence $\sigma_{ph} \propto \sqrt{I}$. For pulsed illumination and TPA, it is reasonable to expect therefore $\sigma_{ph} \propto I$. In addition, direct TPA

excitations of electrons from the VB to Fe^{3+} and Nb_{Li}^{5+} states can not be excluded. However, due to the much smaller density of states compared to the density of states in the CB, we estimate that they play a minor role only. In the qualitative model described here, these transitions do not change the results, but they should be reconsidered for subsequent quantitative statements.

It is worth to mention that in all cases depletion of the writing beam does not play a role: since 285 $m^{-1} \times d$ is just 0.14 and hence much smaller than one, where $d = 0.5$ mm is the thickness of the crystal, we can assume homogeneous illumination along the x-axis for linear absorption and for TPA.

4.3 Charge migration

The bulk photovoltaic effect is the main driving force for the charge redistribution along the c-axis in $LiNbO_3$:Fe, and diffusion can usually be neglected. However, electrons excited from the VB to the CB can not contribute to the bulk photovoltaic current: as it was measured by Krätzig et al. in [21] and [22], the bulk photovoltaic effect vanishes for band-to-band transitions. Gratings created solely by TPA should consequently be based on diffusion only, and therefore be orders of magnitude weaker than gratings based on linear excitation [4]. We observe a decrease of Δn_{sat}, but just by about a factor of two, comparing fs and cw data. Therefore, the bulk photovoltaic effect must still play a role, and electrons are excited from photorefractive centers, namely Nb_{Li}^{4+} and Fe^{2+}. Since these sites are initially mostly unoccupied by electrons in the oxidized crystals, an indirect excitation must occur: part of the electrons excited into the CB by TPA recombine with Nb_{Li}^{5+} or Fe^{3+} and therefore populate these levels, leading to a sensitization of the crystal. From there, the electrons can be excited again and contribute to the bulk photovoltaic current (processes 2 and 3 in Fig. 8).

From our data, we get no indication, which of these two photorefractive centers dominates the process. We know that electrons in the Nb_{Li}^{4+} and Fe^{2+} states have very different lifetimes and therefore different availability for re-excitation, though: for the electron at the Nb_{Li}^{4+} level ("small bound polaron"), a lifetime of up to milliseconds was reported in [23]. Since we see the same intensity dependence of the writing time for 1000 Hz and 33 Hz repetition rate, see Fig. 5(a), we conclude that no significant amount of Nb_{Li}^{4+} polarons exists until the next pulse. The electrons in this level can therefore be re-excited only by light of the same pulse. This might be possible, since the formation of the polarons takes place at or below the timescale of our pulse duration [24]. In contrast, the electrons trapped in iron are much less mobile, and hence their lifetime is larger. In [25], a lifetime of 1 s is reported, limited by the annihilation with slowly moving holes in the VB. Therefore, a re-excitation by subsequent fs pulses is possible.

All excited electrons contribute to the photoconductivity σ_{ph}, but only those electrons, that are trapped at and later re-excited from a photorefractive center, contribute to the bulk photovoltaic current density j_{phv}. Holes and photorefractive centers compete against each other for trapping the excited electrons. With increasing pulse energy, more and more holes are generated simultaneously with the electrons, while the density of the unoccupied photorefractive centers Nb_{Li}^{5+} and Fe^{3+} is at best fixed, or even decreases, since these levels are more and more populated by electrons. Therefore, the *relative* number of excited electrons that recombine with photorefractive centers gets smaller with rising pulse energy. In addition, the larger hole density shortens the lifetime of the electrons in photorefractive centers, since they can more easily find a hole for recombination, decreasing the probability of re-excitation. Hence, the ratio j_{phv}/σ_{ph} will get smaller with rising pulse energy, which is the likely reason for the observed decrease of $\Delta n_{sat}(I)$.

4.4 Final charge trapping

Since we see an electro-optic grating that is stable for many minutes, the final grating must be stored in the $Fe^{2+/3+}$ level: the migration of the electron in process 3 of Fig. 8 leads to a surplus of a negative charge at its new position, which will finally be trapped by an Fe^{3+}, forming Fe^{2+} (process 4 in Fig. 8). At its old position, after the illumination, all holes have to vanish, at least on the timescale of several seconds. Since there is an excess of positive charge at this position, this finally leads to a decrease of the local Fe^{2+} concentration, compared to the initial situation.

After that and integrated over the whole crystal, the number of electrons trapped at Fe sites, i.e. the number of Fe^{2+} states, must reach the initial value. Therefore, only these electrons can contribute to the final charge distribution. There is sufficient Fe^{2+} even in the oxidized samples to explain the observed space charge fields. As complicated the redistribution process of electrons with femtosecond pulses is, in the end it is just a redistribution of electrons between $Fe^{2+/3+}$ sites, like for the photorefractive effect with linear excitations. The other, foregoing processes are only of catalytical nature, accelerating this migration process.

5 Conclusions

When writing gratings into $LiNbO_3$:Fe with femtosecond pulses and cw laser light at a wavelength of 532 nm, two important differences are observed: (1) The saturation refractive index changes decrease for higher peak pulse intensities. (2) While oxidization of the crystals makes writing with cw light much slower, it does almost not affect the

writing with femtosecond pulses. Based on these observations, a basic model of possible charge excitations, redistribution, and trapping is given: it considers in particular two-photon electron–hole excitations and transient trapping of charge carriers at antisite and iron positions, resulting in a sensitization of the material. Re-excitation from these levels, charge migration due to the bulk photovoltaic effect and final trapping by Fe^{2+} ions lead to the observed electro-optic gratings.

Acknowledgements Financial support from the DFG (award BU 913/19-1) and from the Deutsche Telekom AG is gratefully acknowledged. We thank Boris Sturman for helpful comments.

References

1. P. Günter, J.-P. Huignard (eds.), *Photorefractive Materials and Their Applications*, vol. 3 (Springer, New York, 2007)
2. A. Ashkin, G.D. Boyd, J.M. Dziedzic, R.G. Smith, A.A. Ballman, J.J. Levinstein, K. Nassau, Appl. Phys. Lett. **9**, 72 (1966)
3. L. Arizmendi, Phys. Stat. Sol. (a) **201**, 253 (2004)
4. K. Buse, Appl. Phys. B **64**, 273 (1997)
5. K. Buse, Appl. Phys. B **64**, 391 (1997)
6. H.-T. Hsieh, D. Psaltis, O. Beyer, D. Maxein, C. von Korff Schmising, K. Buse, B. Sturman, Opt. Lett. **30**, 2233 (2005)
7. O. Beyer, I. Breunig, F. Kalkum, K. Buse, Appl. Phys. Lett. **88**, 051120 (2006)
8. K. Oba, P.-C. Sun, Y. Fainman, Opt. Lett. **23**, 915 (1998)
9. S. Juodkazis, V. Mizeikis, M. Sudzius, H. Misawa, K. Kitamura, S. Takekawa, E.G. Gamaly, W.Z. Krolikowski, A.V. Rode, Appl. Phys. A **93**, 129 (2008)
10. A.A. Maznev, T.F. Crimmins, K.A. Nelson, Opt. Lett. **23**, 1378 (1998)
11. H. Kogelnik, Bell Syst. Tech. J. **48**, 2909 (1969)
12. G. Peterson, A. Glass, T. Negran, Appl. Phys. Lett. **19**, 130 (1971)
13. H. Kurz, E. Krätzig, W. Keune, H. Engelmann, U. Gonser, B. Dischler, A. Räuber, Appl. Phys. **12**, 355 (1977)
14. J. Bückers, D. Maxein, D. Haertle, K. Buse, J. Opt. Soc. Am. B **26**(5) (2009, to be published)
15. N.V. Kukhtarev, Sov. Tech. Phys. Lett. **2**, 438 (1976)
16. E. Krätzig, R. Orlowski, Ferroelectrics **27**, 241 (1980)
17. F. Jermann, J. Otten, J. Opt. Soc. Am. B **10**, 2085 (1993)
18. M. Simon, S. Wevering, K. Buse, E. Krätzig, J. Phys. D **30**, 144 (1997)
19. O. Beyer, D. Maxein, K. Buse, B. Sturman, H. Hsieh, D. Psaltis, Opt. Lett. **30**, 1366 (2005)
20. G. Montemezzani, P. Dittrich, P. Günter, in *Photorefractive Materials and Their Applications 1—Basic Effects* (Springer, New York, 2006), p. 203, Chap. 7
21. E. Krätzig, H. Kurz, J. Mod. Opt. **24**, 475 (1977)
22. E. Krätzig, H. Kurz, J. Electrochem. Soc. **124**, 131 (1977)
23. P. Herth, D. Schaniel, T. Woike, T. Granzow, M. Imlau, E. Krätzig, Phys. Rev. B **71**, 125128 (2005)
24. O. Beyer, D. Maxein, T. Woike, K. Buse, Appl. Phys. B **83**, 527 (2006)
25. P. Herth, T. Granzow, D. Schaniel, T. Woike, M. Imlau, E. Krätzig, Phys. Rev. Lett. **95**, 067404 (2005)